Supporting Information

Side Chain Isomerization Enables High Efficiency and Thickness Tolerance Organic Solar Cells

Zhixiang Li[‡a], Bailin Zhou[‡a], Shuchao Zhang[‡a], Changzun Jiang[a], Yalu Zou[a], Shitong Li[a], Yang Yang[b], Zhaoyang Yao[a], Xiangjian Wan[a*] and Yongsheng Chen[a*]

[a] *The Centre of Nanoscale Science and Technology and Key Laboratory of Functional Polymer Materials, Institute of Polymer Chemistry, State Key Laboratory of Elemento-Organic Chemistry, College of Chemistry, Renewable Energy Conversion and Storage Center (RECAST), Nankai University, Tianjin 300071, China.*

[b] *The Institute of Seawater Desalination and Multipurpose Utilization, Ministry of Natural Resources (Tianjin), Tianjin 300192, China.*

‡Zhixiang Li, Bailin Zhou and Shuchao Zhang contributed equally to this paper.

*Address correspondence to: xjwan@nankai.edu.cn, yschen99@nankai.edu.cn.

Content

1. Measurements and Instruments

The ^{1}H, ^{13}C nuclear magnetic resonance (NMR) spectra were taken on a Bruker AV400 Spectrometer. Matrix-assisted laser desorption/ionization time-of-flight (MALDI-TOF) mass spectrometry was performed on a Bruker Autoflex III instrument. Fourier transform mass spectrometry (FTMS) with high-resolution matrix-assisted laser desorption/ionization (HR-MALDI) was performed on a Varian 7.0T FTMS instrument. Ultraviolet-visible (UV-*vis*) absorption spectra were measured on a UV-Vis instrument Agilent Cary 5000 UV-vis-NIR spectrophotometer. Ultraviolet photoelectron spectroscopy (UPS) spectra are measured by a Thermo Scientific ESCALAB 250Xi. Cyclic voltammetry (CV) experiments were employed to evaluate the energy levels with an LK98B II Microcomputer-based Electrochemical Analyzer in acetonitrile solution at room temperature. The experiments were carried out in a conventional three-electrode configuration with a glassy carbon electrode as the working electrode, a saturated calomel electrode (SCE) as the reference electrode and a Pt wire as the counter electrode. Tetrabutylammonium phosphorus hexafluoride (Bu_4NPF_6, 0.1 M) in dry acetonitrile solution was used as the supporting electrolyte with the scan rate of 100 mV/s under the protection of nitrogen. The highest occupied molecular orbital (HOMO) and lowest unoccupied molecular orbital (LUMO) energy levels were calculated from the onset oxidation potential and the onset reduction potential, using the equation $E_{HOMO}=-(4.80+E_{ox}^{onset})$, $E_{LUMO}=-(4.80+E_{red}^{onset})$. The thickness of films was measured by Dektak 150 profilometer. The current density-voltage (J-V) curves of photovoltaic devices were recorded by a Keithley 2400 source-measure unit. The photocurrent was measured under the simulated illumination of 100 mW cm^{-2} with AM1.5 G using a Enli SS-F5-3A solar simulator, which was calibrated by a standard Si solar cell (made by Enli Technology Co., Ltd., Taiwan, and calibrated report can be traced to NREL). The thickness of the active layers was measured by a Veeco Dektak 150 profilometer. The EQE spectra were measured by using a QE-R Solar Cell Spectral Response Measurement System (Enli Technology Co., Ltd., Taiwan). Atomic force microscope (AFM) investigation was performed using Bruker

MultiMode 8 in tapping mode. The transmission electron microscopy (TEM) investigation was performed on Philips Technical G2 F20 at 200 kV. Grazing-incidence wide-angle X-ray scattering (GIWAXS) measurement was performed at Xenocs/Xeuss 2.0. The hole and electron mobility were measured using the space charge limited current (SCLC) method, employing a diode configuration of ITO/PEDOT:PSS/active layer/MoO_3/Al for holes and ITO/ZnO/active layer/PDINO/Ag for electrons by taking the dark current density and fitting the results to a space charge limited form, where SCLC is described by:

$$J = \frac{9\varepsilon_0 \varepsilon_r \mu V^2}{8L^3}$$

where J is the current density, L is the film thickness of the active layer, μ is the hole or electron mobility, ε_r is the relative dielectric constant of the transport medium, ε_0 is the permittivity of free space (8.85×10^{-12} F m^{-1}), V ($=V_{appl} - V_{bi}$) is the internal voltage in the device, where V_{appl} is the applied voltage to the device and V_{bi} is the built-in voltage due to the relative work function difference of the two electrodes. Transient photocurrent (TPC) and photovoltage (TPV) measurements were performed on a Molex 180081-4320. Time-of-flight secondary ion mass spectrometry (TOF-SIMS) measurement was performed at PHI Nano TOF II TOF-SIMS (ULVAC-PHI, Japan) with Ar cluster as etching ion species. The films of ITO/ZnO/NMA/PM6:FEH2C8-2Cl with 110 and 300 nm thickness were prepared following the procedure that used to fabricate real devices.

2. Materials Synthesis and Characterization

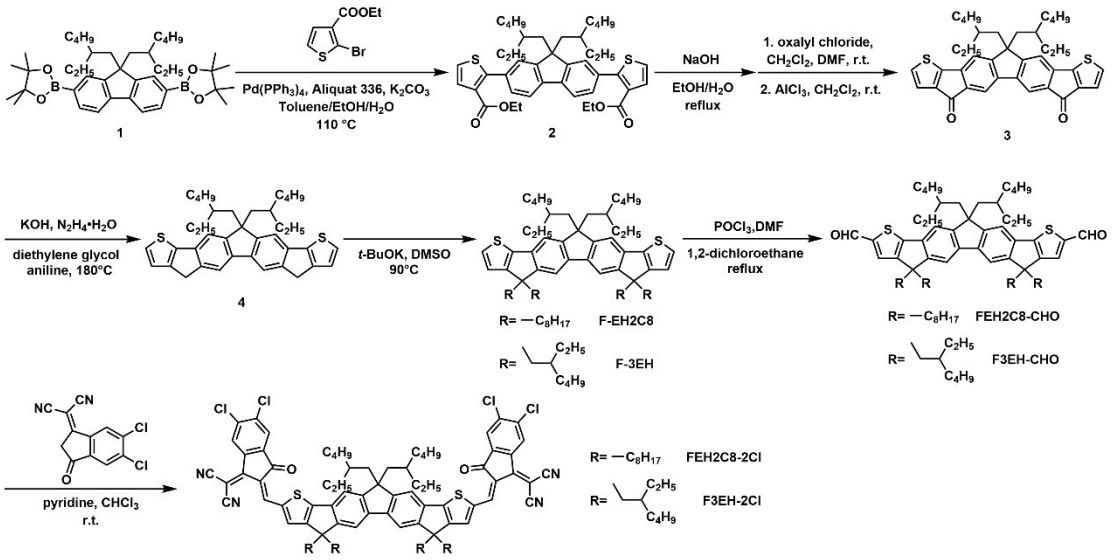

Scheme S1. Synthetic routes to **FEH2C8-2Cl** and **F3EH-2Cl**.

All the raw materials were purchased from commercial suppliers and used directly without further purification. The polymeric donor **PM6** was purchased from Derthon Optoelectronics Materials Science Technology Co LTD. All the reactions and manipulations were performed under the argon atmosphere by using the standard Schlenk techniques due to the high HOMO energy levels of materials.

Synthesis of Compound 2:

2,7-bis(4,4,5,5-tetramethyl-1,3,2-dioxaborolan-2-yl)-9,9-bis(2-ethylhexyl) fluorene (4.75 g, 7.39 mmol), ethyl 2-bromothiophene-3-carboxylate (5.21 g, 22.18 mmol), K_2CO_3 (6.13 g, 44.34 mmol), Aliquat 336 (0.90 g, 2.22 mmol), toluene (50 mL), EtOH (10 mL) and water (10 mL) were added into a 250 mL two-neck flask and degassed with argon for three times. And then tetrakis(triphenylphosphine)palladium (1.71 g, 1.48 mmol) was added into the mixture quickly. The reaction solution was stirred at 110℃ overnight. After cooling down to room temperature, the reaction mixture was poured into water and extracted with dichloromethane for three times. The combined organic layer was dried over anhydrous Na_2SO_4 and filtered. The filtrate was concentrated under vacuum and purified by column chromatography to obtain

compound **2** (5.17 g, 75%). ^{1}H NMR (400 MHz, Chloroform-*d*) δ 7.72 (d, J = 7.8 Hz, 2H), 7.55 – 7.45 (m, 6H), 7.25 (d, J = 5.5 Hz, 2H), 4.30 – 3.99 (m, 4H), 2.08 – 1.93 (m, 4H), 1.22 – 1.13 (m, 6H), 1.10 – 0.70 (m, 18H), 0.69 – 0.63 (m, 6H), 0.56 – 0.49 (m, 6H). ^{13}C NMR (101 MHz, Chloroform-*d*) δ 162.90, 151.24, 150.33, 140.96, 131.86, 129.91, 129.20, 128.19, 125.16, 123.61, 119.00, 60.11, 55.04, 44.27, 34.46, 33.78, 28.10, 26.73, 22.64, 13.97, 13.89, 10.09. MS (MALDI-TOF): calcd for $C_{43}H_{54}O_4S_2$ $[M]^+$, 699.02; found: 699.28.

Synthesis of compound 3:

To a 250 mL two-neck flask was added compound **2** (3.62 g, 5.18 mmol), sodium hydroxide (2.90 g, 72.5 mmol), ethanol (200 mL), and water (30 mL). The reaction mixture was refluxed at 90°C for 12 h. The ethanol was removed under reduced pressure. 1M concentrated HCl was added to acidify the solution. The precipitate was collected by filtration and washed with water.

Then, the residue was mixed with dry dichloromethane (100 mL), oxalyl dichloride (3.38 g, 26.63 mmol) and dry N,N-dimethylformide (1 mL) was slowly added. The mixture was stirred under N_2 at rt for 12 h. The solvent was removed by reduced pressure to yield acid chloride compound as a yellow solid. Without further purification, the residue was dissolved with dry dichloromethane (70 mL). A solution of $AlCl_3$ (2.34 g, 17.55 mmol) in dry dichloromethane (40 mL) was added to the above solution by syringe at 0°C. The mixture was stirred at rt for 3 h. After removal of the solvent by reduced pressure, the residue was extracted with ethyl acetate (100 mL×3) and brine (100 mL × 3). The collected organic layer was dried over $MgSO_4$. After removal of the solvent, the residue was purified by column chromatography on silica gel (hexane/ethyl acetate, v/v, 25/1) to afford a red solid product **3**(1.14 g, 36%). ^{1}H NMR (400 MHz, Chloroform-*d*) δ 7.77 (s, 2H), 7.20 – 7.10 (m, 6H), 2.06 – 1.97 (m, 4H), 0.97 – 0.75 (m, 18H), 0.68 – 0.62 (m, 6H), 0.60 – 0.52 (m, 6H). ^{13}C NMR (101 MHz, Chloroform-*d*) δ 186.63, 159.19, 157.28, 142.55, 140.57, 137.59, 136.43, 128.77, 121.60, 115.52, 115.03, 56.01, 44.19, 34.75, 33.43, 27.99, 26.98, 22.65, 13.95, 10.31. MS (MALDI-TOF): calcd for $C_{39}H_{42}O_2S_2$ $[M]^+$, 606.88; found: 607.21

Synthesis of compound 4:

A mixture of compound **3** (0.50 g, 0.82 mmol), potassium hydroxide (0.92 g, 16.40 mmol) in diethylene glycol (20 mL) and aniline (20 ml) was heated to 100ºC for 30 min. Hydrazine monohydrate (0.82 g, 16.40 mmol) was then slowly added to above solution dropwise. The mixture was heated to 180°C for 24 h. After being cooled to rt, the mixture was quenched by HCl (aq) followed by extraction with ethyl acetate (30 mL×3) and brine (100 mL×1). The collected organic layer was dried over MgSO4. After removal of the solvent, the residue was purified by column chromatography on silica gel (hexane) to yield a white solid **4** (0.33 g, 70%). ^{1}H NMR (400 MHz, Chloroform-*d*) δ 7.77 (s, 2H), 7.55 – 7.50 (m, 2H), 7.35 – 7.30 (m, 2H), 7.16 – 7.11 (m, 2H), 3.75 (s, 4H), 2.16 – 2.08 (m, 4H), 1.44 – 1.21 (m, 4H), 0.96 – 0.85 (m, 14H), 0.71 – 0.65 (m, 6H), 0.61 – 0.54 (m, 6H). ^{13}C NMR (101 MHz, Chloroform-*d*) δ 149.16, 146.10, 144.28, 142.85, 137.79, 136.19, 125.15, 121.81, 114.90, 113.34, 53.29, 43.86, 33.57, 32.82, 32.50, 27.00, 25.96, 21.73, 12.93, 9.26. MS (MALDI-TOF): calcd for $C_{39}H_{46}S_2$ $[M]^+$, 578.92; found: 579.31.

Synthesis of F-EH2C8:

A solution of **4** (0.3 g, 0.52 mmol) in dry DMSO (20 mL) was heated at 80°C. ^{t}BuOK (0.58 g, 5.18 mmol) dissolved in dry DMSO (30 mL) was added to the above mixture. After the reaction mixture was stirred at 80ºC for 1 h, 1-bromo-2-ethylhexane (0.80 g, 4.15 mmol) was added dropwise. The mixture was further stirred at 90ºC for 4 h. The reaction was quenched by ice water and extracted with dichoromethane. After being dried over Na_2SO_4, the organic layer was removed by reduced pressure and the residue was simply purified by column chromatography on silica gel (petroleum ether) to afford a sticky yellow product **F-EH2C8**. The excess alkyl bromide and the product are difficult to separate, we did a crude NMR characterization and MS characterization, and then the products would be used for the next step. The excess alkyl bromide does not affect the next reaction.

Synthesis of FEH2C8-CHO:

$POCl_3$ (2 mL) was added dropwise to DMF (5 mL) at 0°C under the protection of argon and then stirred at room temperature for 3 h to obtain the Vilsmeier reagent. Then it was added into a 1,2-dichloroethane (DCE) (40 mL) solution of compound **F-**

EH2C8. The above reaction mixture was stirred at room atmosphere for 1 h and then heated to 80°C for overnight. The mixture was quenched by saturated NaOAc in ice water, and then extracted with DCM (50 mL×3). The combined organic layer was dried over anhydrous Na_2SO_4. The organic layer was removed by reduced pressure and the residue was purified by column chromatography on silica gel to afford a yellow oil **FEH2C8-CHO** (0.29 g, 52% yield). ^{1}H NMR (400 MHz, Chloroform-*d*) δ 9.90 (s, 2H), 7.68 – 7.61 (m, 4H), 7.55 –7.49 (m, 2H), 2.12 – 1.92 (m, 12H), 1.21 – 1.07 (m, 40H), 0.88 – 0.68 (m, 38H), 0.59 – 0.54 (m, 6H), 0.50 – 0.44 (m, 6H). ^{13}C NMR (101 MHz, Chloroform-*d*) δ 182.73, 155.33, 154.56, 152.16, 151.21, 144.96, 141.19, 135.67, 130.29, 116.10, 113.84, 54.35, 54.05, 44.67, 39.19, 34.76, 33.41, 31.66, 29.88, 29.18, 29.03, 28.04, 27.16, 24.09, 22.46, 13.95, 10.48. MS (MALDI-TOF): calcd for $C_{73}H_{110}O_2S_2$ $[M]^+$, 1083.80; found: 1083.80.

Synthesis of F3EH-CHO:

The synthesis route is same as that of **FEH2C8-CHO**, except that 2-ethylhexyl bromide was used to replace 1-bromo-2-ethylhexane to afford **F3EH-CHO** (43% yield). ^{1}H NMR (400 MHz, Chloroform-*d*) δ 9.90 (s, 2H), 7.72 – 7.61 (m, 4H), 7.53 (s, 2H), 2.13 – 1.96 (m, 12H), 0.90 – 0.43 (m, 90H). ^{13}C NMR (101 MHz, Chloroform-*d*) δ 182.83, 155.16, 154.42, 152.21, 151.32, 144.69, 140.87, 136.13, 131.25, 116.06, 114.76, 54.56, 53.94, 44.35, 35.02, 34.76, 34.30, 33.78, 29.68, 28.57, 28.12, 26.85, 22.71, 14.13, 13.99, 10.56, 10.11. MS (MALDI-TOF): calcd for $C_{73}H_{110}O_2S_2$ $[M]^+$, 1083.80; found: 1083.04.

Synthesis of FEH2C8-2Cl:

Under the protection of argon, compound **FEH2C8-CHO** (0.2 g, 0.18 mmol) and 2-(5,6-dichlorine-3-oxo-2,3-dihydro-1H-inden-1-ylidene) malononitrile (**INIC-2Cl**) (0.29 g, 1.11 mmol) was dissolved in dry CF (50 mL), followed by the addition of pyridine (0.6 mL). After stirring at 35℃ for 12 h, the mixture was concentrated in vacuum. MeOH (50 mL) was poured into the residues. The crude was precipitated and filtered through qualitative filter paper. Then the residue was dissolved in chloroform. The solvent was removed by reduced pressure and further purified by silica gel and

then recrystallized from CF/hexane/CH_3OH to give **FEH2C8-2Cl** as a dark blue solid (0.19 g, 65% yield). ^{1}H NMR (400 MHz, Chloroform-*d*) δ 9.01 (s, 2H), 8.79 (s, 2H), 7.96 (s, 2H), 7.75 (s, 2H), 7.73 – 7.69 (m, 4H), 2.15 – 1.96 (m, 12H), 1.21 – 1.05 (m, 40H), 0.91 – 0.69 (m, 38H), 0.61 – 0.56 (m, 6H), 0.54 – 0.49 (m, 6H). ^{13}C NMR (101 MHz, Chloroform-*d*) δ 186.11, 163.56, 158.47, 157.12, 156.47, 152.68, 152.40, 152.12, 143.11, 139.48, 139.23, 138.60, 136.24, 136.04, 126.91, 125.08, 120.20, 117.53, 114.58, 114.44, 68.80, 54.52, 54.31, 44.83, 39.36, 34.92, 33.53, 31.70, 29.91, 29.25, 28.08, 27.15, 24.29, 22.51, 13.98, 10.51. HR-MS: calcd for $C_{97}H_{114}Cl_4N_4O_2S_2$ $[M]^+$, 1573.9250; found: 1573.7221.

Synthesis of F3EH-2Cl:

The synthesis route is same as that of **FEH2C8-2Cl**, yielding 64%. ^{1}H NMR (400 MHz, Chloroform-*d*) δ 9.00 (s, 2H), 8.79 (s, 2H), 7.96 (s, 2H), 7.82 – 7.68 (m, 6H), 2.21 – 1.98 (m, 12H), 1.08 – 0.35 (m, 90H). ^{13}C NMR (101 MHz, Chloroform-*d*) δ 186.20, 163.20, 158.48, 157.12, 156.23, 152.36, 142.58, 140.27, 139.55, 139.28, 139.16, 138.67, 136.68, 136.13, 126.96, 125.08, 120.51, 117.33, 115.45, 114.46, 69.13, 54.70, 54.07, 44.63, 43.86, 35.20, 34.81, 33.84, 29.70, 28.60, 28.04, 26.82, 22.79, 14.04, 10.51, 10.10. HR-MS: calcd for $C_{97}H_{114}Cl_4N_4O_2S_2$ $[M]^+$, 1573.9250; found: 1573.7171.

3. Device Fabrication

The OSCs were fabricated by applying an inverted architecture of ITO/ZnO/NMA/active layer/MoO_3/Ag. Firstly, the indium tin oxide (ITO) glass substrates were cleaned by ultrasonic treatment in detergent, deionized water, acetone, and isopropyl alcohol in turn for 15 min and subsequently dried by use of an argon blow. Subsequently, the ZnO was deposited by spin-coating a ZnO precursor solution on the top of ITO glass substrates at 3000 rpm for 20 s. After being baked at 200 °C in the air for 40 min, the ZnO-coated substrates were transferred into an argon-filled glove box. In order to fine-tune the interfacial properties, a thin film of NMA was spin-coated on ZnO. Subsequently, the PM6:F-2Cl/FEH2C8-2Cl/F3EH-2Cl (1:1, *w/w*, D: 9 mg/mL) in chlorobenzene (CB) with DIO additive contents (0.5% for PM6:FEH2C8-2Cl and 0.3% for another) was spin-coated at 1600 rpm onto the NMA layer. Then, MoO_3 (~6 nm) and Ag (~150 nm) were successively evaporated onto the active layer through a shadow mask ($2x10^{-4}$ Pa). The effective area for the devices is 4 mm^2.

The large-area modules were fabricated with an architecture similar to that of the small-area cells. ITO-coated glass substrates were rinsed by ultrasonic treatment in detergent, deionized water, acetone, and isopropyl alcohol in turn for 15 min and subsequently dried by use of an argon blow. After that, the ZnO layer was blade-coated on precleaned ITO-coated glass with a coating velocity of 10 mm/s and a blade–substrate gap of 200 μm. After being baked at 200°C in the air for 40 min, a thin film of NMA was blade-coated on ZnO with a coating velocity of 10 mm/s and a blade–substrate gap of 150 μm. The PM6:FEH2C8-2Cl (1:1, w/w, D: 9 mg/mL) in chlorobenzene with 0.5 vol% DIO was blade-coated with a coating velocity of 20 mm/s and a blade–substrate gap of 400 μm in air. Then, MoO_3 (~6 nm) and Ag (~150 nm) were successively evaporated onto the active layer through a shadow mask ($2x10^{-4}$ Pa). The effective area for the devices is 25 cm^2. And the thickness of active-layer was tested to be around 200 nm by using step profiler.

4. Figures and Tables

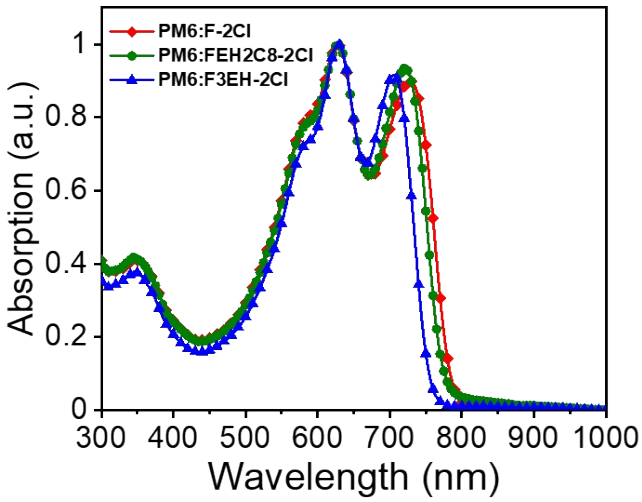

Figure S1. UV-vis absorption spectra of the blend films of PM6:F-2Cl, PM6:FEH2C8-2Cl and PM6:F3EH-2Cl under their respective optimal device conditions.

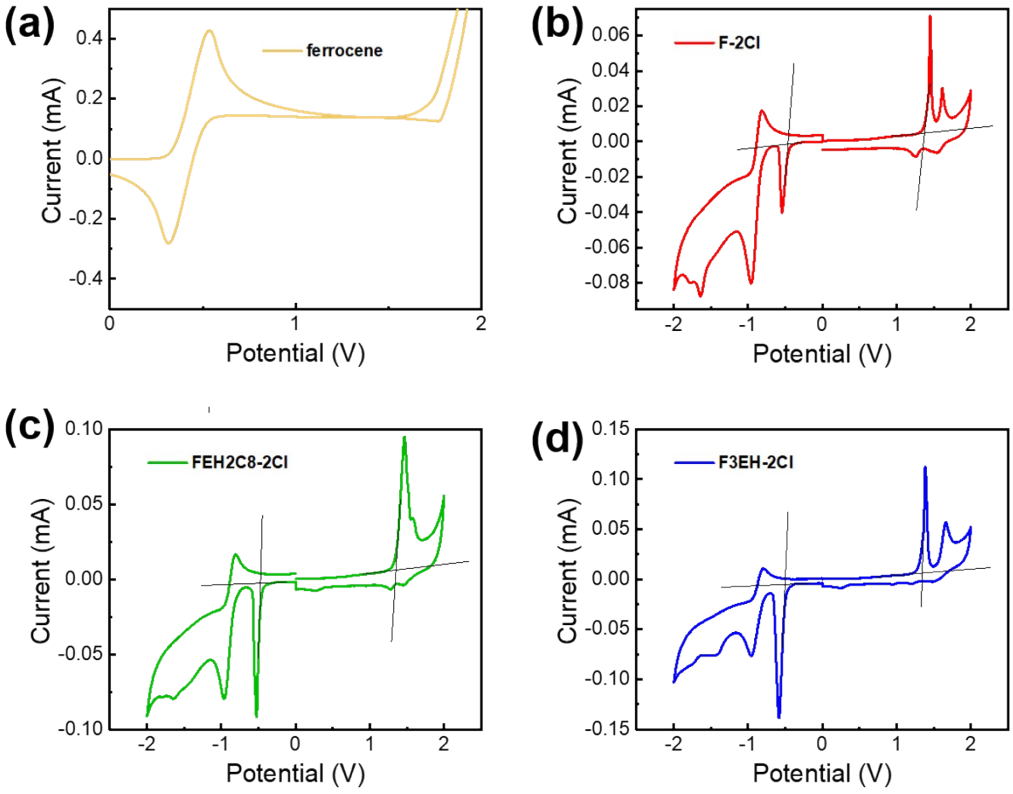

Figure S2. Cyclic voltammetry plots of (b) F-2Cl, (c) FEH2C8-2Cl and (d) F3EH-2Cl.

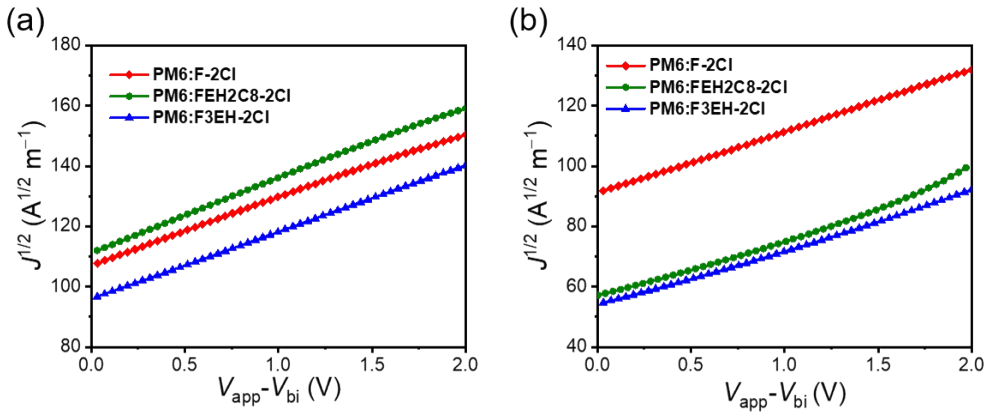

Figure S3. The electron (a) and hole (b) mobilities of optimized devices.

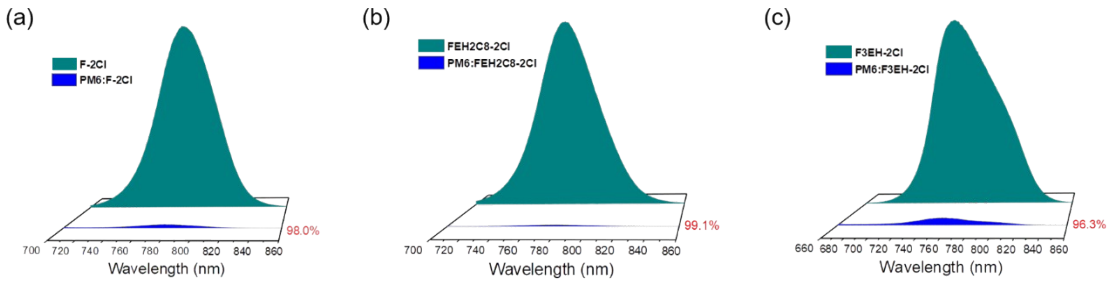

Figure S4. The PL spectrum of the neat and blend films.

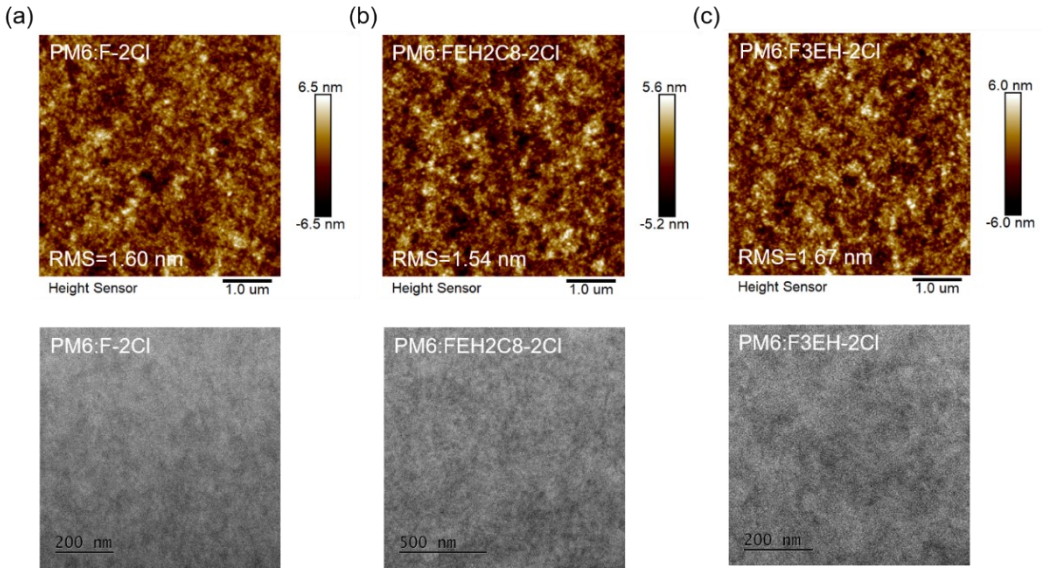

Figure S5. Atomic force microscopy (AFM) height images and transmission electron microscopy (TEM) of (a) PM6:F-2Cl, (b) PM6:FEH2C8-2Cl and (c) PM6:F3EH-2Cl blend films.

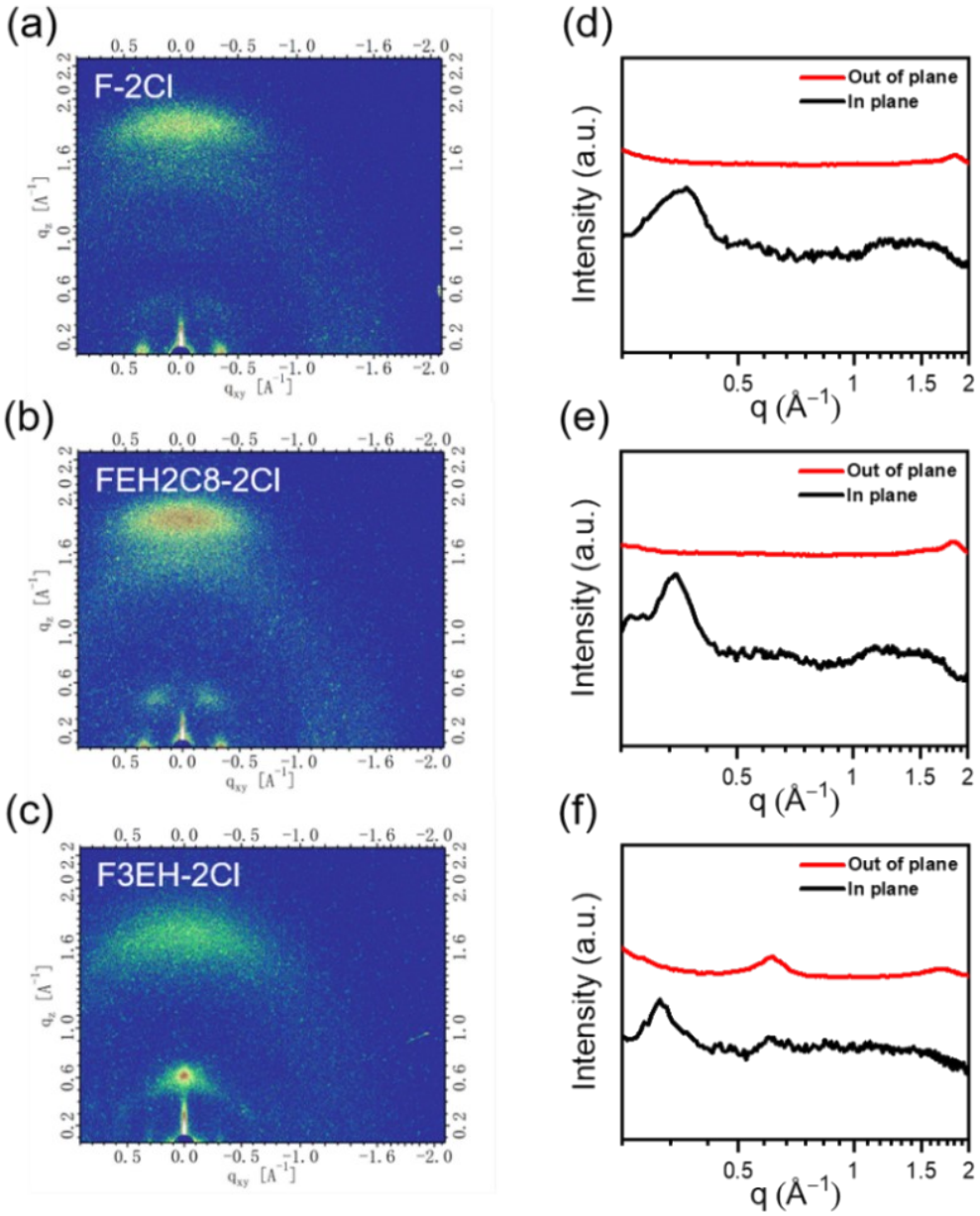

Figure S6. 2D GIWAXS patterns and for (a) F-2Cl, (b) FEH2C8-2Cl and (c) F3EH-2Cl neat films. GIWAXS scattering profiles cut of (d) F-2Cl, (e) FEH2C8-2Cl and (f) F3EH-2Cl neat films.

Table S1. Photovoltaic performance of the solar cells based on PM6:FEH2C8-2Cl with different thermal annealing temperature under the illumination of AM 1.5G, 100 mW cm^{-2}.

Thermal annealing (TA) [°C]	V_{oc} [V]	J_{sc} [mA cm^{-2}]	FF [%]	PCE [%]
None	0.917	19.16	77.62	13.64
80	0.912	19.62	77.89	13.94
100	0.910	19.97	78.24	14.22
120	0.897	20.20	78.27	14.18

Table S2. Photovoltaic performance of the solar cells based on PM6:FEH2C8-2Cl (100℃ annealing) with different D: A ratios under the illumination of AM 1.5G, 100 mW cm^{-2}.

D/A [w/w]	V_{oc} [V]	J_{sc} [mA cm^{-2}]	FF [%]	PCE [%]
1:0.8	0.915	18.93	78.01	13.51
1:1	0.910	19.97	78.24	14.22
1:1.2	0.906	19.96	77.40	14.00

Table S3. Photovoltaic performance of the solar cells based on PM6:FEH2C8-2Cl (1:1, *w/w*) with different DIO contents under the illumination of AM 1.5G, 100 mW cm^{-2}.

V%	V_{oc} [V]	J_{sc} [mA cm^{-2}]	FF [%]	PCE [%]
0.3	0.913	19.66	77.17	13.85
0.5	0.918	20.12	79.04	14.60
0.7	0.915	19.96	78.93	14.42

Table S4. Photovoltaic performances of the solar cells based on PM6:FEH2C8-2Cl (1:1, *w/w*, 0.5% DIO) with different thermal annealing temperature under the illumination of AM 1.5G, 100 mW cm^{-2}.

Thermal annealing (TA) [°C]	V_{oc} [V]	J_{sc} [mA cm^{-2}]	FF [%]	PCE [%]
None	0.918	20.12	79.04	14.60
80	0.908	19.79	77.46	13.92
100	0.901	19.53	78.01	13.73

Table S5. Photovoltaic performance of the solar cells based on PM6:F3EH-2Cl with different thermal annealing temperature under the illumination of AM 1.5G, 100 mW cm^{-2}.

Thermal annealing (TA) [°C]	V_{oc} [V]	J_{sc} [mA cm^{-2}]	FF [%]	PCE [%]
None	0.963	17.82	75.35	12.93
80	0.953	18.52	75.39	13.31
100	0.948	18.64	74.99	13.25
120	0.933	18.87	73.25	12.90

Table S6. Photovoltaic performance of the solar cells based on PM6:F3EH-2Cl (80°C annealing) with different D: A ratios under the illumination of AM 1.5G, 100 mW cm^{-2}.

D/A [w/w]	V_{oc} [V]	J_{sc} [mA cm^{-2}]	FF [%]	PCE [%]
1:0.8	0.962	18.15	73.30	12.80
1:1	0.953	18.52	75.39	13.31
1:1.2	0.944	18.77	74.56	13.21

Table S7. Photovoltaic performance of the solar cells based on PM6:F3EH-2Cl (1:1, *w/w*) with different DIO contents under the illumination of AM 1.5G, 100 mW cm^{-2}.

V%	V_{oc} [V]	J_{sc} [mA cm^{-2}]	FF [%]	PCE [%]
0.15	0.948	18.92	74.04	13.28
0.3	0.952	18.99	76.25	13.79
0.5	0.943	18.53	75.13	13.13

Table S8. Photovoltaic performances of the solar cells based on PM6:F3EH-2Cl (1:1, *w/w*, 0.3% DIO) with different thermal annealing temperature under the illumination of AM 1.5G, 100 mW cm^{-2}.

Thermal annealing (TA) [°C]	V_{oc} [V]	J_{sc} [mA cm^{-2}]	FF [%]	PCE [%]
None	0.952	18.99	76.25	13.79
80	0.940	18.50	76.03	13.22
100	0.935	18.32	76.41	13.09

Table S9. Summary of SCLC mobility measurements.

Device	μ_h[×10^{-4} cm^{2}V^{-1}s^{-1}]	μ_e[×10^{-4} cm^{2}V^{-1}s^{-1}]	μ_h/μ_e
PM6:F-2Cl	3.01	2.38	1.26
PM6:FEH2C8-2Cl	3.40	2.87	1.18
PM6:F3EH-2Cl	2.86	1.96	1.46

Table S10. Summary of the GIWAXS parameters for the neat acceptor films and blend films.

Film	IP		OOP		
	q (Å^{-1})	d (Å)	q (Å^{-1})	d (Å)	CCL (Å)
F-2Cl	0.37	17.15	1.83	3.44	37.20
FEH2C8-2Cl	0.35	18.16	1.83	3.43	37.77
F3EH-2Cl	0.31	20.16	1.73	3.63	19.68
PM6:F-2Cl	0.31	20.05	1.78	3.54	27.79
PM6:FEH2C8-2Cl	0.30	20.61	1.79	3.51	28.06
PM6:F3EH-2Cl	0.29	21.09	1.76	3.56	20.45

Table S11. Photovoltaic parameters of PM6-based binary OSCs with FF over 79%.

Active layer	V_{OC} [V]	J_{SC} [mA cm^{-2}]	FF [%]	PCE [%]	Refs.
PM6:MF1	0.914	16.67	79.37	12.09	1
PM6:PDFC	0.97	15.93	81.3	12.56	2
PM6:IDIC-C5Ph	0.948	19.19	80.02	14.56	3
PM6:IT-4F	0.87	20.73	80.79	14.57	4
PM6:WA1	0.860	22.65	79.31	15.45	5
PM6:BTP-ClBr	0.906	23.48	79.0	16.82	6
PM6:BTP-eC9	0.839	26.2	81.1	17.8	7

PM6:BTP-4F-P2EH	0.880	25.85	80.08	18.22	8
PM6:L8-BO	0.87	25.72	81.5	18.32	9
PM6:EH-HD-4F	0.84	27.5	79.3	18.38	10
PM6:AC9	0.871	26.75	79	18.43	11
This work	0.918	20.12	79.04	14.60	

Table S12. Photovoltaic parameters of the large area OSCs with PCE over 10% and area over 20 cm^2.

Modules	Area [cm^2]	PCE^L [%]	PCE^S [%]	PCE^L/PCE^S	Refs.
TPD-3F:IT-4F	20.4	10.4	13.8	0.754	12
PM6:BTP-4Cl-12	25.42	12.42	/	/	13
PM6:Y6	36	13.47	16.26	0.828	14
PM6:BTP-eC9	25.21	14.07	16.33	0.862	15
PV2300:PVA3:$PC_{61}BM$	32.6	10.3	16.1	0.640	16
PCE10:COi8DFIC:$PC_{71}BM$	25	10.09	12.37	0.816	17
PM6:Y6:$PC_{71}BM$	26.75	14.35	/	/	18
PM6:Y6:$PC_{71}BM$	54	13.2	/	/	19
PM6:Y6:$PC_{60}BM$	204	11.7	/	/	20
PM6:Y6:BTO:$PC_{71}BM$	36	14.26	17.41	0.819	21
This work	25	11.71	14.60	0.802	

^{L}PCE of the large area module; ^{S}PCE of the corresponding small-area device.

5. NMR and HR-MS Spectra

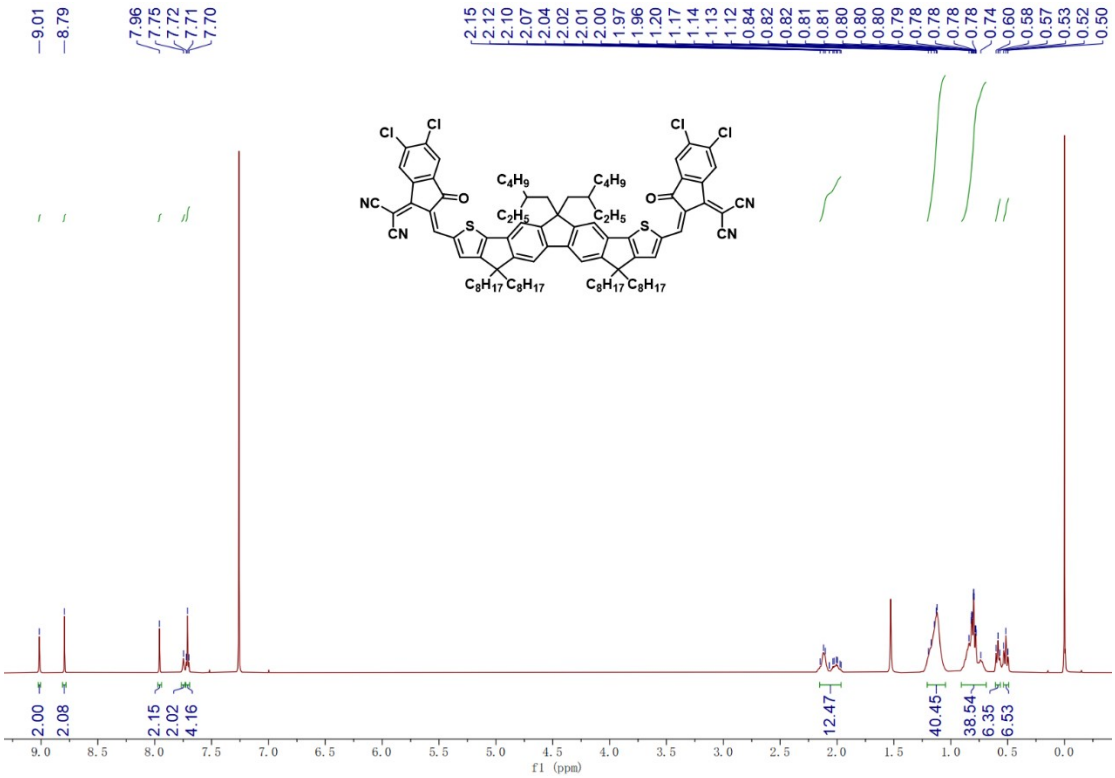

Figure S7. ^{1}H NMR (400 MHz) of compound **FEH2C8-2Cl**.

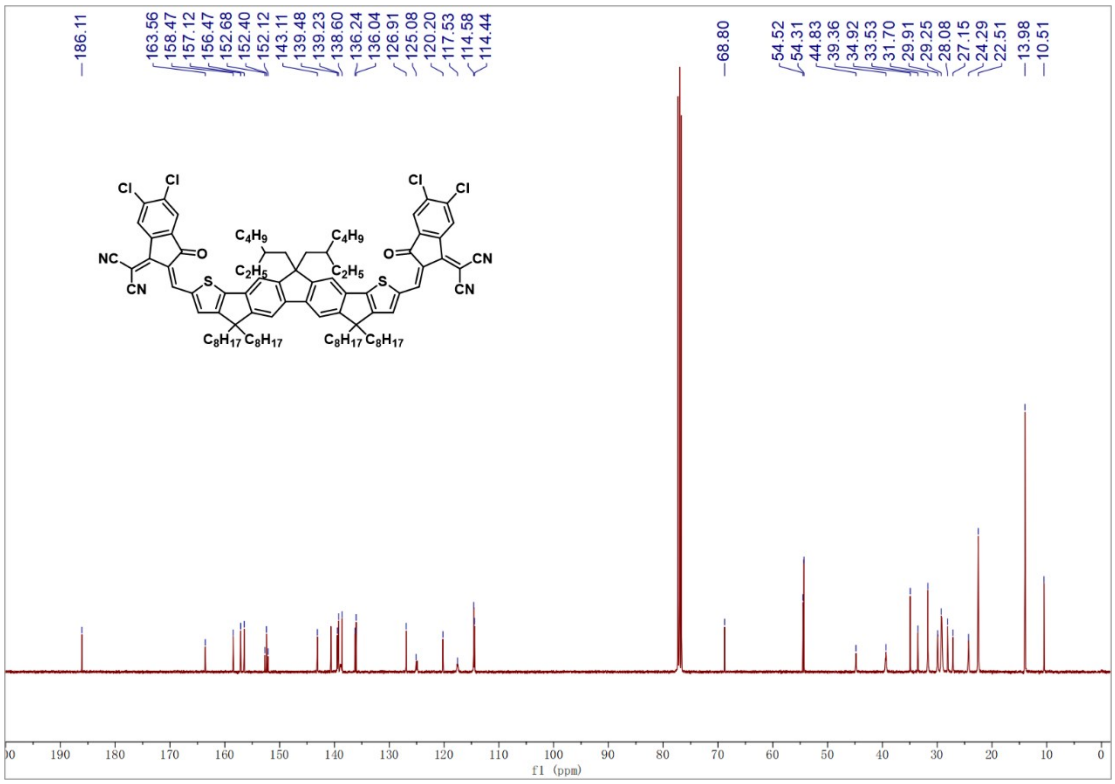

Figure S8. ^{13}C NMR (101 MHz) of compound **FEH2C8-2Cl**.

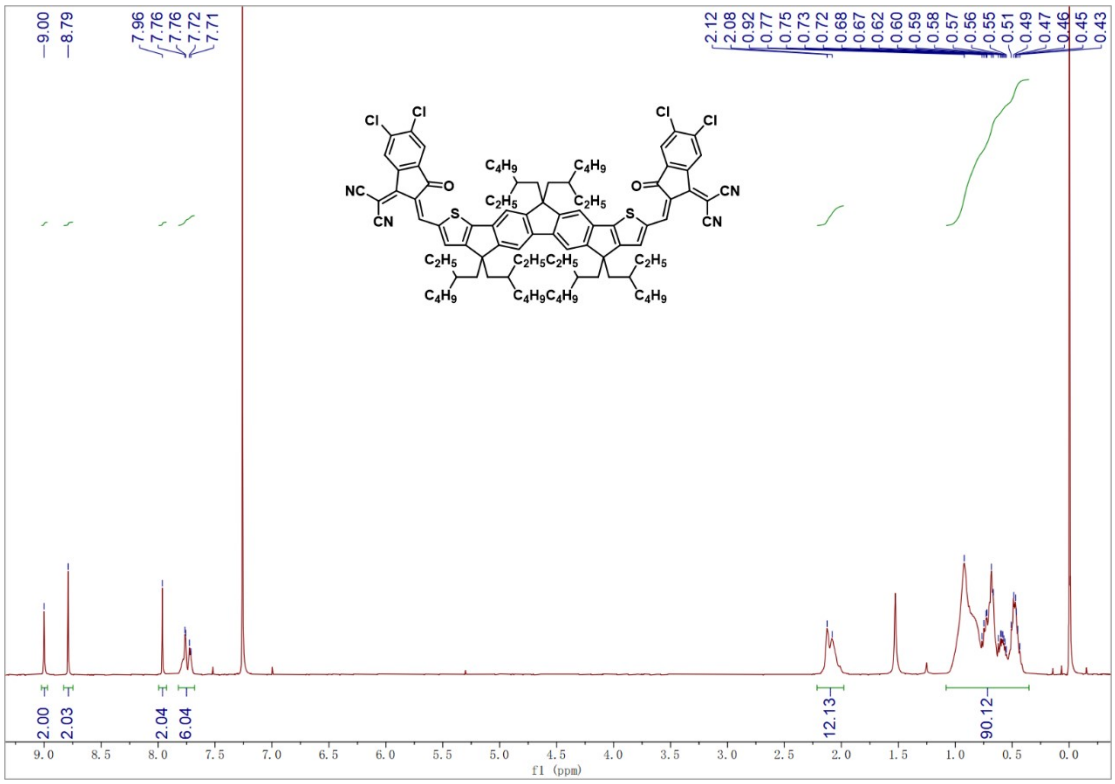

Figure S9. ^{1}H NMR (400 MHz) of compound **F3EH-2Cl**.

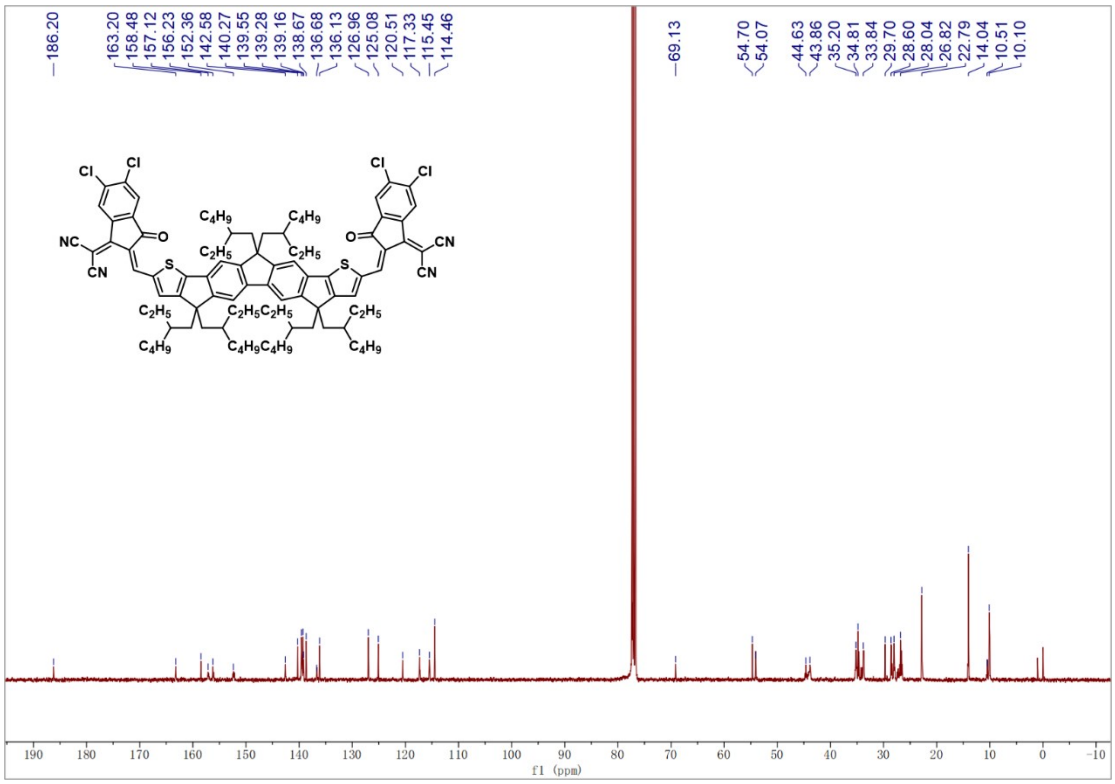

Figure S10. ^{13}C NMR (101 MHz) of compound **F3EH-2Cl**.

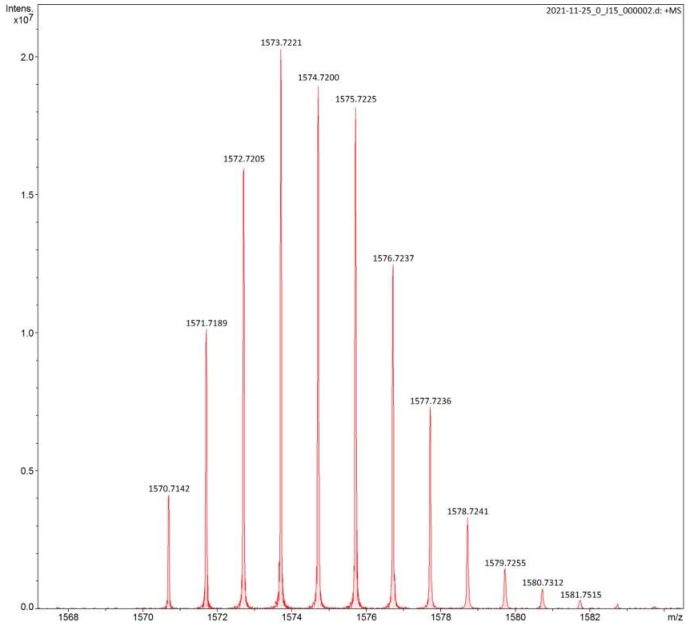

Figure S11. HR-MS spectrum of compound **FEH2C8-2Cl**.

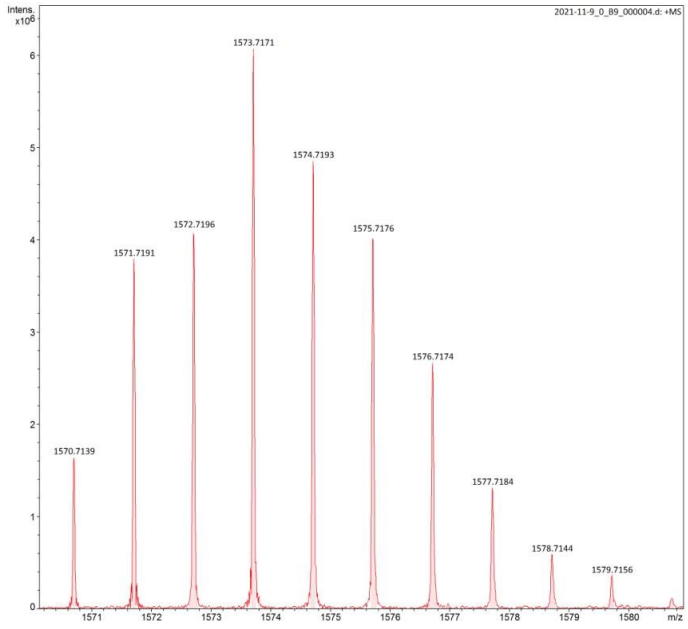

Figure S12. HR-MS spectrum of compound **F3EH-2Cl**.

6. Supplementary References

1. Q. An, J. Wang, W. Gao, X. Ma, Z. Hu, J. Gao, C. Xu, M. Hao, X. Zhang, C. Yang and F. Zhang, *Sci. Bull.*, 2020, **65**, 538-545.
2. K. Ding, T. Shan, J. Xu, M. Li, Y. Wang, Y. Zhang, Z. Xie, Z. Ma, F. Liu and H. Zhong, *Chem. Commun.*, 2020, **56**, 11433-11436.
3. Y. Li, L. Yu, L. Chen, C. Han, H. Jiang, Z. Liu, N. Zheng, J. Wang, M. Sun, R. Yang and X. Bao, *Innovation*, 2021, **2**, 100090.
4. Z. Zheng, Q. Hu, S. Zhang, D. Zhang, J. Wang, S. Xie, R. Wang, Y. Qin, W. Li, L. Hong, N. Liang, F. Liu, Y. Zhang, Z. Wei, Z. Tang, T. P. Russell, J. Hou and H. Zhou, *Adv. Mater.*, 2018, e1801801.
5. P. Wang, Y. Li, C. Han, J. Wang, F. Bi, N. Zheng, J. Yang, J. Wang and X. Bao, *J. Mater. Chem. A.*, 2022, **10**, 17808-17816.
6. Z. Luo, R. Ma, Z. Chen, Y. Xiao, G. Zhang, T. Liu, R. Sun, Q. Zhan, Y. Zou, C. Zhong, Y. Chen, H. Sun, G. Chai, K. Chen, X. Guo, J. Min, X. Lu, C. Yang and H. Yan, *Adv. Energy. Mater.*, 2020, **10**.
7. Y. Cui, H. Yao, J. Zhang, K. Xian, T. Zhang, L. Hong, Y. Wang, Y. Xu, K. Ma, C. An, C. He, Z. Wei, F. Gao and J. Hou, *Adv. Mater.*, 2020, **32**, e1908205.
8. J. Zhang, F. Bai, I. Angunawela, X. Xu, S. Luo, C. Li, G. Chai, H. Yu, Y. Chen, H. Hu, Z. Ma, H. Ade and H. Yan, *Adv. Energy. Mater.*, 2021, **11**, 2102596.
9. C. Li, J. Zhou, J. Song, J. Xu, H. Zhang, X. Zhang, J. Guo, L. Zhu, D. Wei, G. Han, J. Min, Y. Zhang, Z. Xie, Y. Yi, H. Yan, F. Gao, F. Liu and Y. Sun, *Nat. Energy*, 2021, **6**, 605-613.
10. S. Chen, L. Feng, T. Jia, J. Jing, Z. Hu, K. Zhang and F. Huang, *Sci. China Chem.*, 2021, **64**, 1192-1199.
11. C. He, Z. Bi, Z. Chen, J. Guo, X. Xia, X. Lu, J. Min, H. Zhu, W. Ma, L. Zuo and H. Chen, *Adv. Funct. Mater.*, 2022, **32**, 2112511.
12. C. Liao, Y. Chen, C. Lee, G. Wang, N. Teng, C. Lee, W. Li, Y. Chen, C. Li, H. Ho, P. H. Tan, B. Wang, Y. Huang, Ryan M. Young, Michael R. Wasielewski, Tobin J. Marks, Y. Chang and F. Antonio, *Joule*, 2020, **4**.

13. Y. Han, Z. Hu, W. Zha, X. Chen, L. Yin, J. Guo, Z. Li, Q. Luo, W. Su and C. Ma, *Adv. Mater.*, 2022, **34**, 2110276.
14. B. Zhang, F. Yang, S. Chen, H. Chen, G. Zeng, Y. Shen, Y. Li and Y. Li, *Adv. Funct. Mater.*, 2022, **32**, 2202011.
15. X. Dong, Y. Jiang, L. Sun, F. Qin, X. Zhou, X. Lu, W. Wang and Y. Zhou, *Adv. Funct. Mater.*, 2021, 202110209.
16. C. Liao, Y. Hsiao, K. Tsai, N. Teng, W. Li, J. Wu, J. Kao, C. Lee, C. Yang, H. Tan, K. Chung and Y. Chang, *Solar RRL*, 2021, **5**, 2000749.
17. G. Wang, J. Zhang, C. Yang, Y. Wang, Y. Xing, M. A. Adil, Y. Yang, L. Tian, M. Su, W. Shang, K. Lu, Z. Shuai and Z. Wei, *Adv. Mater.*, 2020, 202005153.
18. E. Feng, Y. Han, J. Chang, H. Li, K. Huang, L. Zhang, Q. Luo, J. Zhang, C. Ma, Y. Zou, L. Ding and J. Yang, *J. Semicond*, 2022, **43**, 100501.
19. F. Qin, L. Sun, H. Chen, Y. Liu, X. Lu, W. Wang, T. Liu, X. Dong, P. Jiang, Y. Jiang, L. Wang and Y. Zhou, *Adv. Mater.*, 2021, **33**, e2103017.
20. A. Distler, C. J. Brabec and H. J. Egelhaaf, *Progress in Photovoltaics: Research and Applications*, 2020, **29**, 24-31.
21. H. Chen, R. Zhang, X. Chen, G. Zeng, K. Libor, A. Sabina, B. Zhang, W. Chen, G. Xu, J. Oh, K. So-Huei, S. Chen, C. Yang, J. Brus, J. Hou, F. Gao, Y. Li and Y. Li, *Nat. Energy*, 2021, **6**, 1045–1053